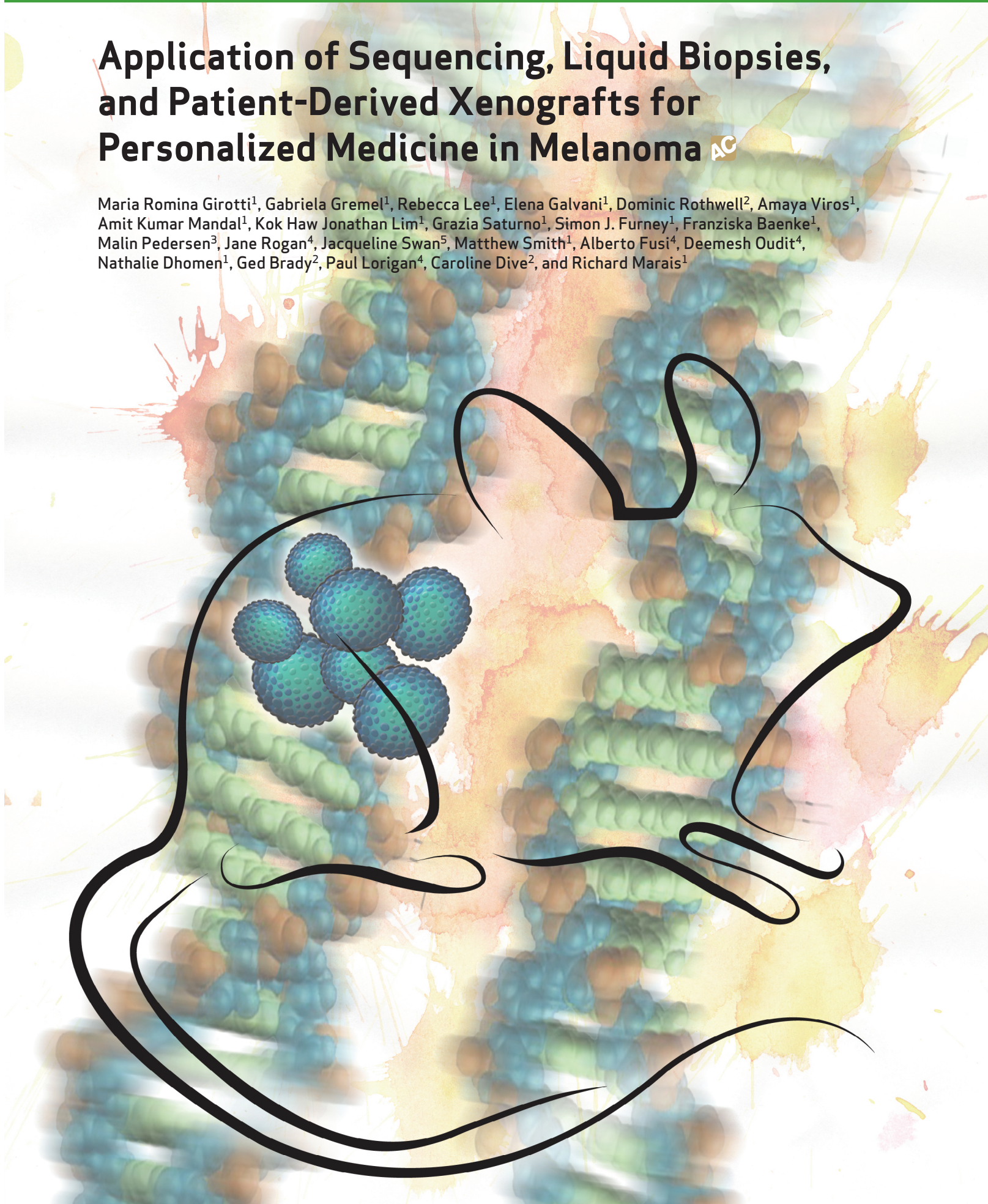


RESEARCH ARTICLE

Application of Sequencing, Liquid Biopsies, and Patient-Derived Xenografts for Personalized Medicine in Melanoma

Maria Romina Girotti¹, Gabriela Gremel¹, Rebecca Lee¹, Elena Galvani¹, Dominic Rothwell², Amaya Viros¹, Amit Kumar Mandal¹, Kok Haw Jonathan Lim¹, Grazia Saturno¹, Simon J. Furney¹, Franziska Baenke¹, Malin Pedersen³, Jane Rogan⁴, Jacqueline Swan⁵, Matthew Smith¹, Alberto Fusi⁴, Deemesh Oudit⁴, Nathalie Dhomen¹, Ged Brady², Paul Lorigan⁴, Caroline Dive², and Richard Marais¹



ABSTRACT

Targeted therapies and immunotherapies have transformed melanoma care, extending median survival from ~9 to over 25 months, but nevertheless most patients still die of their disease. The aim of precision medicine is to tailor care for individual patients and improve outcomes. To this end, we developed protocols to facilitate individualized treatment decisions for patients with advanced melanoma, analyzing 364 samples from 214 patients. Whole exome sequencing (WES) and targeted sequencing of circulating tumor DNA (ctDNA) allowed us to monitor responses to therapy and to identify and then follow mechanisms of resistance. WES of tumors revealed potential hypothesis-driven therapeutic strategies for *BRAF* wild-type and inhibitor-resistant *BRAF*-mutant tumors, which were then validated in patient-derived xenografts (PDX). We also developed circulating tumor cell-derived xenografts (CDX) as an alternative to PDXs when tumors were inaccessible or difficult to biopsy. Thus, we describe a powerful technology platform for precision medicine in patients with melanoma.

SIGNIFICANCE: Although recent developments have revolutionized melanoma care, most patients still die of their disease. To improve melanoma outcomes further, we developed a powerful precision medicine platform to monitor patient responses and to identify and validate hypothesis-driven therapies for patients who do not respond, or who develop resistance to current treatments. *Cancer Discov*; 6(3); 286–99. ©2015 AACR.

INTRODUCTION

Malignant melanoma is the most deadly skin cancer, and each year, there are over 76,000 melanoma cases and 10,000 deaths in the United States (1) and over 100,000 cases and 22,000 deaths in Europe (2). A paradigm shift has occurred in melanoma treatment in the last 5 years. Improved understanding of the genetic landscape of melanoma has facilitated development of effective targeted therapies, and improved knowledge of the molecular controls of the immune system has driven the development of immune checkpoint inhibitors. However, not all patients benefit from these treatments, and resistance is a persistent problem.

The *BRAF* oncogene is mutated in ~50% of melanomas, and although *BRAF* and *MEK* inhibitors increase survival in these patients (3–5), even when they are combined most patients develop resistance after 6 to 12 months (6–8). Antibody antagonists of *CTLA-4* and *PD-1* provide survival benefits in a subset of patients (9–11) and even better responses when combined (10, 11). However, it is unclear which patients will benefit from these agents, so the identification of biomarkers

of response is a priority (12, 13). Moreover, most patients derive little benefit from *CTLA-4* immune checkpoint inhibitors after *BRAF* inhibitors (14), and resistance to targeted therapies is driven by several mechanisms (9). Currently, there are no guidelines or biomarkers to assist in the selection of second-line therapies, so selecting follow-up treatments for patients is challenging. One option is to continue treatment beyond progression (15), but it is unclear which patients will benefit. Furthermore, patients with melanoma lacking a *BRAF* mutation have fewer therapeutic options and are currently limited to chemotherapy or immunotherapy, so additional treatment options are needed for these patients.

Recent advances in DNA-sequencing technologies provide unprecedented capacity to characterize comprehensively the genetic alterations and pathways in tumors, raising the possibility of developing therapies based on the genetic makeup of each tumor (16). The Genomics of Drug Sensitivity in Cancer Project at the Sanger Institute is an example of a large-scale drug screen that incorporates genomic and gene expression data to identify drug response biomarkers that could inform optimal application of cancer drugs (17, 18).

In melanoma, acquired resistance to systemic treatment appears to be driven by clonal evolution and selection of resistant tumor cells (19). Repeated biopsies to study genomic alterations resulting from therapies are invasive, can be difficult to obtain, and may be confounded by intratumoral heterogeneity. A possible resolution to this problem is analysis of circulating tumor DNA (ctDNA) released by cancer cells into the plasma (20). Serial analysis of ctDNA can be used to track genomic evolution of metastatic cancers in response to therapy to complement invasive biopsy approaches and identify mutations associated with acquired drug resistance in advanced cancers (21), but it is unclear how this technology can be used in the routine setting of a hospital. Patient-derived xenografts (PDX) also have the potential to assist personalized medicine decisions (22), but their development requires access to tumor tissue that is often inaccessible or

¹Molecular Oncology Group, Cancer Research UK Manchester Institute, Manchester, United Kingdom. ²Clinical and Experimental Pharmacology Group, Cancer Research UK Manchester Institute, Manchester, United Kingdom. ³Targeted Therapy Team, The Institute of Cancer Research, London, United Kingdom. ⁴The University of Manchester, The Christie NHS Foundation Trust, Manchester, United Kingdom. ⁵Research Services, Cancer Research UK Manchester Institute, Manchester, United Kingdom.

Note: Supplementary data for this article are available at Cancer Discovery Online (<http://cancerdiscovery.aacrjournals.org/>).

M.R. Girotti and G. Gremel contributed equally to this article.

Corresponding Author: Richard Marais, Cancer Research UK Manchester Institute, The University of Manchester, 550 Wilmslow Road, Manchester M20 4BX, United Kingdom. Phone: 44-161-346-3101; Fax: 44-161-918-7491; E-mail: richard.marais@cruk.manchester.ac.uk

doi: 10.1158/2159-8290.CD-15-1336

©2015 American Association for Cancer Research.

accessible only by invasive biopsies. One solution to this challenge is to develop xenografts from circulating tumor cells (CTC), so-called CTC-derived xenografts (CDX), recently developed for small cell lung cancer (SCLC; ref. 23) but not yet for melanoma.

We have developed a platform of technologies for personalized medicine in patients with melanoma by exploiting technical advances in sequencing and xenografts to monitor responses to treatment and explore new treatment options and describe results from our collection of 364 samples from 214 patients with advanced melanoma.

RESULTS

ctDNA Reveals Patient Responses to Treatment

We collected plasma samples from 101 patients with melanoma being treated as part of clinical trials or receiving current standards of clinical care to determine if ctDNA analysis can be used to support clinical diagnostics. The patients presented stage II, III, or IV cutaneous, acral, mucosal, or uveal melanoma, were 26 to 89 years old, and received treatments including chemotherapy, targeted therapies, and immunotherapy (Fig. 1A; Supplementary Table S1). Most patients are still alive and in some cases have been followed for over a year (Fig. 1A; Supplementary Table S1).

Our initial studies were retrospective, as in patient 1 who presented with *BRAF*^{V600E} metastatic melanoma with spread to the lymph nodes and lung (Fig. 1B). The patient presented a partial response to dabrafenib/trametinib, but relapsed at ~23 weeks (Fig. 1B). Accordingly, the *BRAF*^{V600E} ctDNA levels initially fell with tumor shrinkage, but increased again on relapse (Fig. 1B). The patient did not respond to ipilimumab and this was also reflected in the *BRAF*^{V600E} ctDNA levels. Note that serum lactate dehydrogenase (LDH) did not reflect tumor responses (Fig. 1B). Finally, whole exome sequencing (WES) of the patient's resistant tumor revealed an *NRAS*^{Q61R} mutation (Supplementary Fig. S1) that could be detected retrospectively in the patient's ctDNA from week 25 (Fig. 1B).

We also performed prospective studies. Patient 2 presented with rapidly progressing metastatic *BRAF*^{V600R} melanoma in the liver, hepatic, and peritoneal lymph nodes (Fig. 1C). Ipilimumab was ineffective, but there was a dramatic response to dabrafenib/trametinib, with tumor shrinkage in multiple lesions (Fig. 1C). The *BRAF*^{V600R} ctDNA analysis predicted the failure of ipilimumab 1 week before the CT scan, and the response to dabrafenib/trametinib 6 weeks before the CT scan, whereas serum LDH failed to predict these responses (Fig. 1C).

Another example of ctDNA predicting clinical response was seen with patient 3, who presented with metastatic *BRAF*^{V600E} melanoma in the lymph nodes and lung. After one cycle of ipilimumab, treatment was halted due to toxicities that needed to be managed by immunosuppression, allowing

a second cycle of ipilimumab at week 5. *BRAF*^{V600E} ctDNA at 3 and 5 weeks predicted an exceptional response, confirmed by CT scan at week 8 (Fig. 1D). The patient continues to respond and the *BRAF*^{V600E} ctDNA levels remain low at week 17. Note, however, that counter to the clinical response, serum LDH remains high, likely due to mycophenolate mofetil, which was administered for immunosuppressive therapy and is known to raise LDH (24).

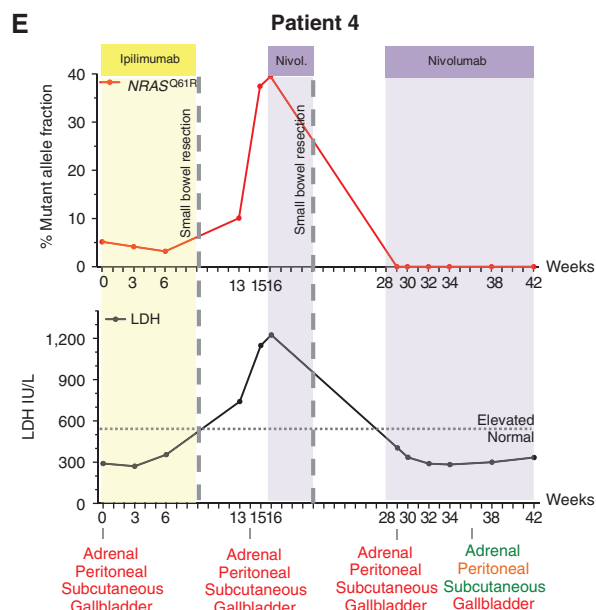
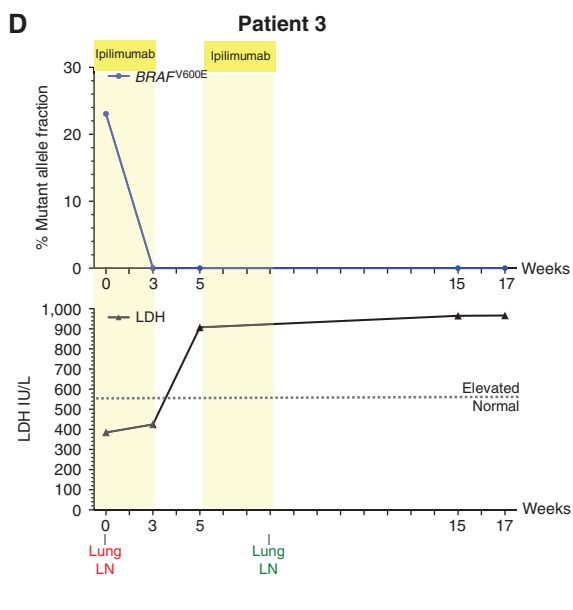
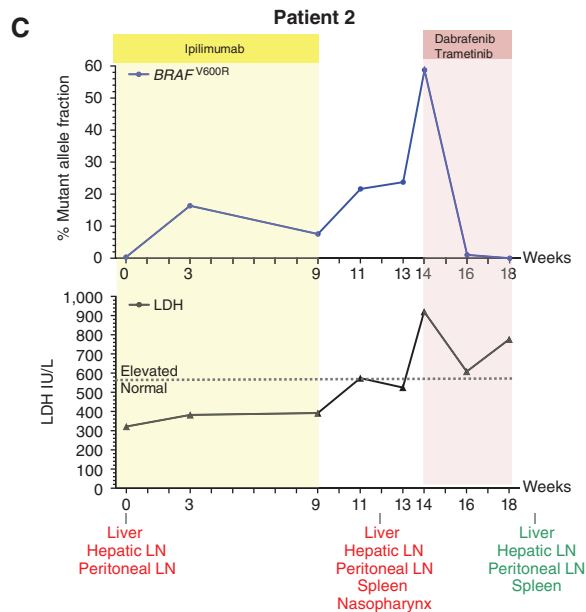
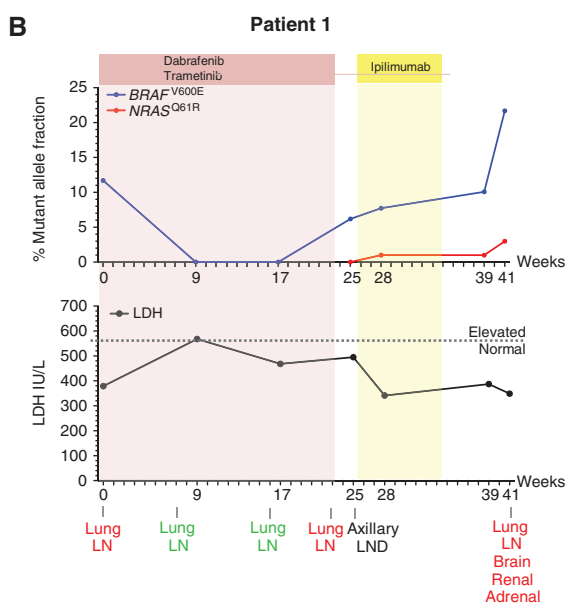
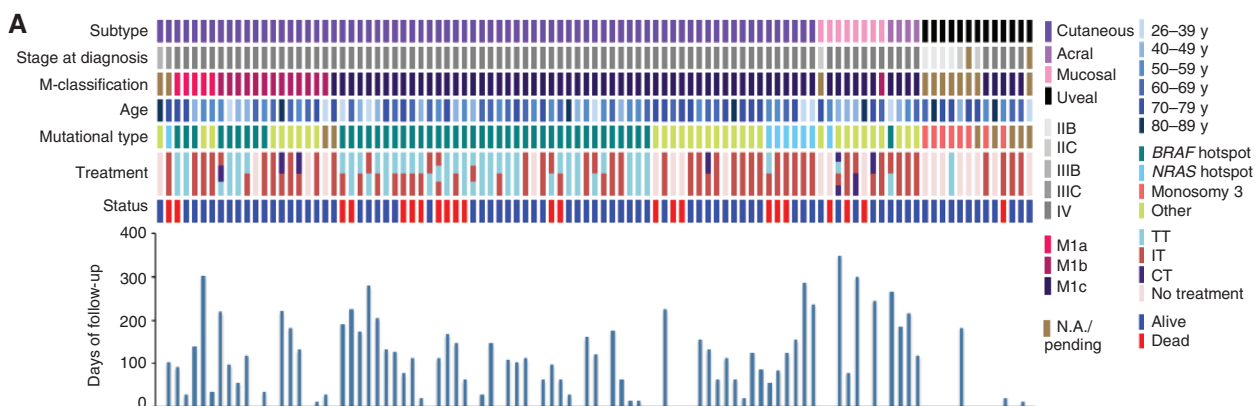
Finally, patient 4 shows an example of a delayed immunotherapy response that was preempted by ctDNA analysis. The patient presented with a jejunal mass that caused intussusception and required resection. *NRAS*^{Q61R} ctDNA analysis at week 13 predicted a failure to respond to ipilimumab, and this was confirmed a week later by a CT scan (Fig. 1E). Nivolumab was administered at week 16 but interrupted briefly due to a small bowel resection at week 20. *NRAS*^{Q61R} ctDNA and serum LDH were both low from week 28, whereas a CT scan at week 28 revealed disease progression (Fig. 1E). Note however that *NRAS*^{Q61R} ctDNA and serum LDH remained low up to week 42, and a CT scan at week 36 revealed that some lesions responded to treatment. Thus, even in this patient the ctDNA analysis was predictive of clinical response.

Targeted Sequencing of ctDNA Reveals Mechanisms of Resistance to Therapy

We also investigated if WES of ctDNA could reveal mechanisms of resistance to therapy. Our first studies were retrospective, as in patient 5, who was previously treated with lymphadenectomy for stage III disease and re-presented with isolated metastatic disease in the lung and was treated by pneumonectomy (Fig. 2A). Seventeen weeks later, new subcutaneous, liver, and brain metastases developed that initially responded to vemurafenib, but then relapsed during the period from weeks 18 to 40. Following a short-lived clinical response to dabrafenib/trametinib, treatment was halted at week 50, and the patient died at week 54. The *BRAF*^{V600E} ctDNA was predictive of the initial response, protracted relapse to vemurafenib, and the short-lived response to dabrafenib/trametinib, whereas serum LDH predicted only the late-stage relapse to dabrafenib/trametinib (Fig. 2A). To determine the mechanism of resistance to vemurafenib, we performed WES of the ctDNA sample at week 50. This revealed an *NRAS*^{Q61K} mutation (Fig. 2B) that was not present at baseline, but emerged at the onset of resistance at week 26 (Fig. 2A).

For routine monitoring of common mechanisms of resistance, we developed a targeted sequencing panel of 10 loci known to mediate resistance to BRAF and MEK inhibitors, using a multiplexed PCR reaction to enrich target DNA regions (Fig. 2C and Supplementary Table S2). Patient 6 presented with stage IV disease with brain, lung, and omental metastases. Vemurafenib and dabrafenib/trametinib were administered with brief interruptions to sustain BRAF/MEK

Figure 1. ctDNA can be used to monitor patient response. **A**, overview of 101 patients with cutaneous, acral, mucosal, and uveal melanoma at different disease stages monitored by circulating free DNA technologies (see Supplementary Materials for more information on melanoma patient sample classification). **B**, time courses for *BRAF*^{V600E} variant allele fractions (VAF; blue), *NRAS*^{Q61R} VAF (red), and serum LDH (black) in patient 1. **C**, time courses for *BRAF*^{V600R} VAF (blue) and serum LDH (black) in patient 2. **D**, time courses for *BRAF*^{V600E} VAF (blue) and serum LDH (black) in patient 3. **E**, time courses for *NRAS*^{Q61R} VAF (red) and serum LDH (black) in patient 4. LDH > 550 IU/L = elevated LDH < 550 IU/L = normal; red organ denomination = progressive disease; orange = stable disease; green = response; N.A., not available; TT, targeted therapy; IT, immunotherapy; CT, chemotherapy; LN, lymph node; LND, lymph node dissection.



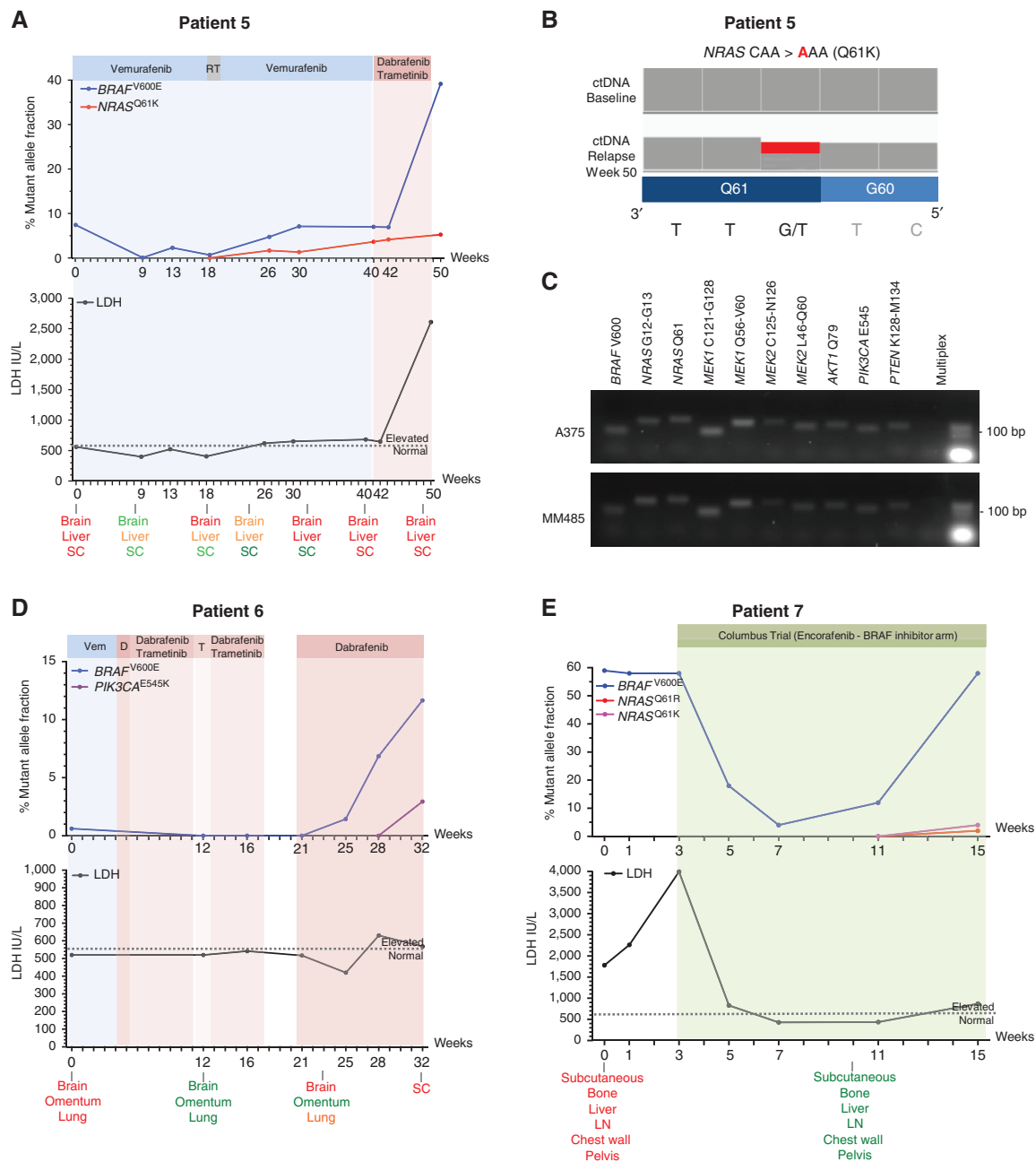


Figure 2. ctDNA can be used to monitor response and emerging resistance in patients with melanoma on targeted therapy. **A**, time courses for BRAF^{V600E} VAF (blue), NRAS^{Q61K} VAF (red), and serum LDH (black) in patient 5. **B**, Integrative Genomics Viewer (IGV) visualization for WES of codon Q61 of NRAS in the baseline versus 50-week relapsed ctDNA sample. The red color indicates the G>T transition for the p.Q61K mutation in the tumor. **C**, 10-loci primer panel for targeted sequencing analysis of the ctDNA. Individual primers were tested using chromosomal DNA isolated from two melanoma cell lines, A375 and MM485. **D**, time courses for BRAF^{V600E} VAF (blue), PIK3CA^{E545K} VAF (purple), and serum LDH (black) in patient 6. **E**, time courses for BRAF^{V600E} VAF (blue), NRAS^{Q61R} VAF (red), NRAS^{Q61K} VAF (pink), and serum LDH (black) in patient 7. LDH > 550 IU/L = elevated LDH < 550 IU/L = normal; RT, radiotherapy; SC, subcutaneous; D, dabrafenib; T, trametinib; Vem, vemurafenib; LN, lymph node.

inhibition while managing toxicities (Fig. 2D). A CT scan at week 12 revealed a good partial response and the BRAF^{V600E} ctDNA remained below detection limits. A second scan at week 23 revealed ongoing abdominal response but slow progression in the brain. The BRAF^{V600E} ctDNA revealed disease progression at week 25, which was clinically confirmed at week 28 (Fig. 2D; Supplementary Fig. S2A). Targeted

sequencing of the ctDNA revealed a *de novo* PIK3CA^{E545K} mutation that emerged coincident with resistance to dabrafenib at week 32 (Fig. 2D) when treatment was withdrawn, followed by death at week 36.

Finally, patient 7 presented with aggressive disease with multiple subcutaneous, liver, and bone metastases, abdominal lymphadenopathy, a pelvic mass, and peritoneal thickening (Fig. 2E).

The patient received encorafenib (LGX818) monotherapy as part of a clinical trial (NCT01090453), and serum LDH and ctDNA at weeks 5 and 7 suggested a partial response that was confirmed by CT scan at week 10 (Fig. 2E). *BRAF*^{V600E} ctDNA analysis at week 11 revealed that relapse was occurring, and this was substantiated by clinical examination at week 15 and was coincident with a further increase of *BRAF*^{V600E} and the appearance of *NRAS*^{Q61R} and *NRAS*^{Q61K}, revealing the likely mechanisms of resistance (Fig. 2E; Supplementary Fig. S2B). A CT scan at week 18 confirmed disease progression, demonstrating that for this patient, the ctDNA analysis provided an early warning of relapse 7 weeks before it was confirmed by the scan.

A PDX Collection to Guide Clinical Care of Patients with Melanoma

We showed earlier that longitudinal analysis of ctDNA is a powerful approach to monitor patient responses to immunotherapies and targeted therapies. Moreover, ctDNA can be used to reveal mechanisms of resistance in individual patients. To complement ctDNA analysis with a strategy for selecting second-line therapeutic options, we developed a systematic pipeline to establish melanoma PDXs, implanting 126 samples from 120 patients with cutaneous, acral, and uveal melanoma into NOD.Scid IL2 γ (NSG) mice (Fig. 3A). The samples were derived from subcutaneous sites, lymph nodes, and visceral metastases, and we also established PDXs from pleural effusions, ascites, and a primary uveal melanoma from an enucleated eye (Fig. 3A). The patients were all stage III or IV, but many stage III patients progressed to stage IV over the course of the study (Fig. 3A). They ranged from 25 to 95 years and they were treatment naïve or had received typical treatments, including chemotherapy, targeted therapy, and immunotherapy (Fig. 3A). Our success rate for PDX engraftment was 72% with median latency to 100 mm³ of 49 days, and, as many patients were followed for up to 12 months (Fig. 3A; Supplementary Table S3), we had ample opportunity to develop and test clinically relevant personalized treatments for individual patients.

We exemplify our approach with patient 5, for whom we developed a PDX from the pneumonectomy previously described (Fig. 3B; see also Fig. 2A). The PDX retained the histologic features of the patient's tumor (Fig. 3C), and WES revealed extensive overlap in the single nucleotide variants (SNV) of the patient's tumor and PDX, and also confirmed the presence of *BRAF*^{V600E} (Fig. 3D). Concurrent with the patient's treatment with vemurafenib, mice bearing the PDX were treated with PLX4720, a vemurafenib analogue with superior oral bioavailability in mice (25, 26). In parallel with the patient, the mice initially responded, but complete regression was not achieved and resistance emerged after 12 to 16 weeks (Fig. 3E and Supplementary Fig. S3). The patient was judged unlikely to benefit from ipilimumab, radiotherapy, or surgery, and WES did not reveal new actionable therapeutic targets in the resistant PDX (data not shown), leaving dabrafenib plus trametinib as the patient's only treatment option. The preferred treatment option was a combination of dabrafenib and trametinib, although it was understood that any benefit would be short-lived (27). At the time, this combination was available only through an Expanded Access Program (EAP) in the United Kingdom, but the patient was

ineligible for this program due to the brain lesions. However, we found that the PLX4720-resistant PDX responded briefly (~10 weeks) to dabrafenib/trametinib (Fig. 3F), and used these data to obtain permission from the sponsor for this combination in the patient. As in the mice, the patient received a brief (8-week) clinical benefit from the combination, showing that PDX technology can be used to refine patient care.

BRAF Inhibitor Treatment Past Progression Induces Growth and Metastasis in a Drug-Resistant Tumor

Clinicians currently face a difficult decision as to whether to continue to treat beyond progression patients who relapse on targeted therapy with the hope of slowing tumor growth, or whether to halt targeted therapy and consider alternatives. We illustrate this problem in patient 8, who developed inoperable axillary nodal disease that carried a *BRAF*^{V600E} mutation. The patient received vemurafenib, and after 12 weeks a 50% reduction in tumor volume enabled complete resection of the lesion (Fig. 3G). Vemurafenib was not provided after surgery due to a lack of evidence for benefit from adjuvant therapy, but the patient relapsed with metastatic disease, and although vemurafenib was readministered at week 24, the disease progressed rapidly and the patient died at week 37 (Fig. 3G).

We established two PDXs from this patient, one from the tumor removed at week 12 and one from a pleural effusion drained at week 37 (Fig. 3G), providing a rare pair of responding and relapsing tumors from the same patient. Critically, PLX4720 accelerated the growth of the 12-week PDX (Fig. 3H) and we observed micrometastatic lesions in the lungs of PLX4720-treated mice bearing the 12-week PDX, but not the vehicle-treated controls (Fig. 3I). WES of the 12-week tumor revealed an *NRAS*^{Q61K} mutation that was not present in the biopsy taken at presentation (Fig. 3J), and this mutation was further enriched in the 37-week pleural effusion PDX (Fig. 3K). Thus, consistent with our previous cell line studies (28, 29), BRAF inhibition accelerated the growth and metastasis in this *NRAS* mutant PDX, suggesting that treatment beyond progression was inappropriate for the patient and highlighting how improved knowledge of melanoma biology could assist with decisions about when to continue and when to withdraw treatment.

Identification and Validation of Treatments for Non-V600 Mutant BRAF Patients

Current treatments for non-V600 mutant *BRAF* patients are based on immunotherapy and chemotherapy, but ~50% of patients do not respond. A key challenge for personalized medicine is therefore to develop treatments for these patients, so we tested if this could be achieved by combining next-generation sequencing and PDX technologies. We sequenced 80 patient tumors by WES or by targeted sequencing with a panel of 40 melanoma driver genes and genes known to be drivers of resistance to targeted therapy (Supplementary Table S4; refs. 30–32). Forty-eight tumors carried V600 *BRAF* mutations and one a K601 mutation (Fig. 4A), all of which are activating and known to respond to BRAF inhibitors (33). Nineteen tumors carried *RAS* mutations, three carried *NFI* mutations, and nine were wild-type for *BRAF*, *NRAS*, and *NFI* (Fig. 4A). We observed several significantly mutated genes

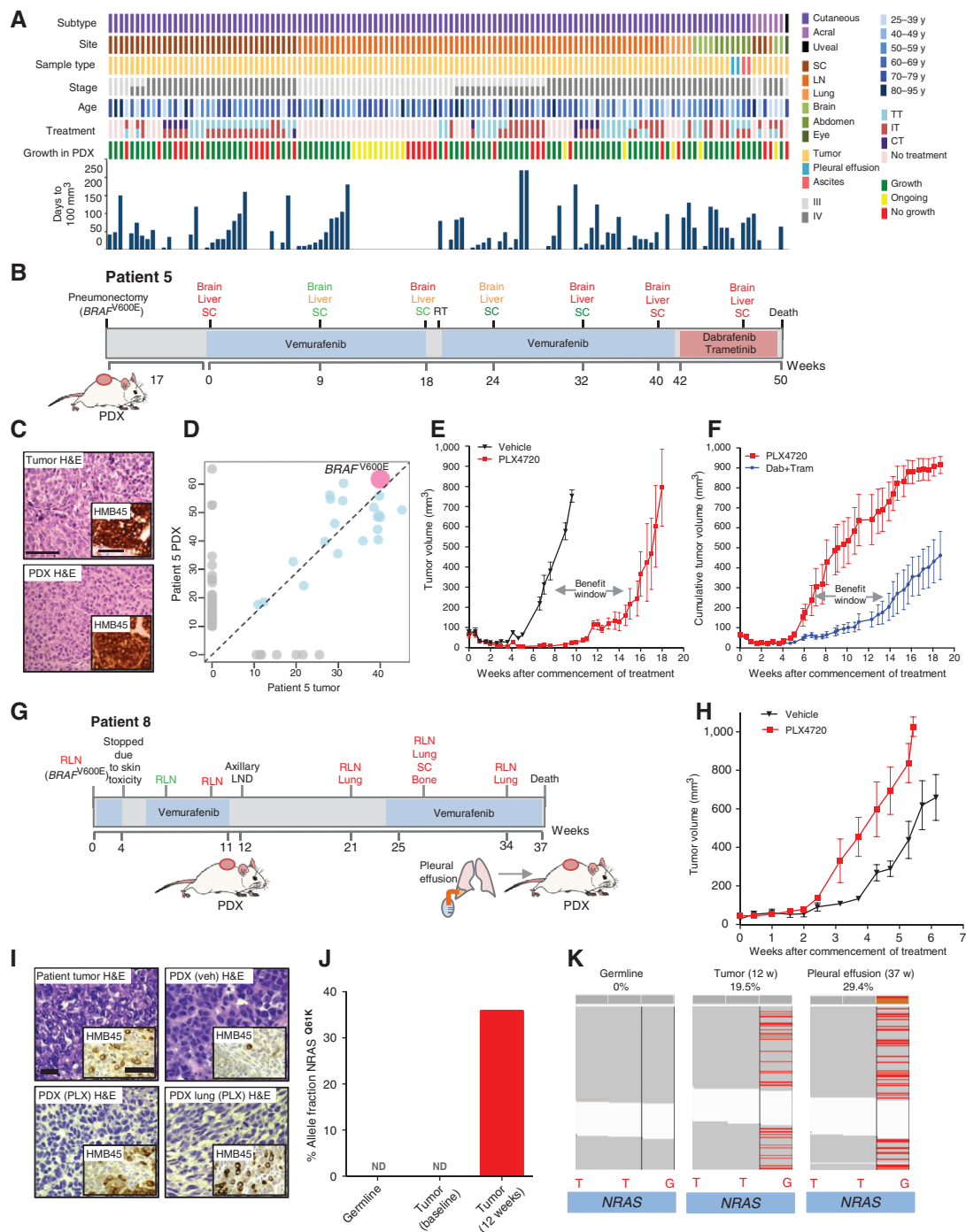


Figure 3. PDX technologies to refine patient care. **A**, overview of 126 stage III and IV cutaneous, acral, and uveal melanoma patient samples implanted into NSG mice to establish PDXs (see Supplementary Materials for more information on melanoma patient sample classification). **B**, patient 5 clinical history. **C**, photomicrographs showing hematoxylin and eosin (H&E) staining of the tumor from patient 5 (top) and the corresponding PDX (bottom). Inset, melanoma-specific antibody HMB45/MelanA staining. Scale bar, 100 μ m. **D**, SNV correlation in the tumor from patient 5 and the corresponding PDX. Gray dots, private SNVs; blue dots, shared SNVs; pink dot, BRAF^{V600E}. Dotted line, ideal fit. Pearson product-moment correlation; $P < 2.2e-16$; $r^2 = 0.68$. **E**, growth of patient 5 PDX in mice treated with vehicle or PLX4720 (45 mg/kg/d orally). Mean tumor volumes \pm SEM ($n = 5$ per group) are shown. **F**, growth of PLX4720-resistant patient 5 PDX from **E** in mice treated with PLX4720 (45 mg/kg/d orally) or dabrafenib (25 mg/kg/d orally)/trametinib (0.15 mg/kg/d orally). Drug treatments commenced immediately after reimplant from **E** and show mean tumor volumes \pm SEM ($n = 9$ per group). **G**, patient 8 clinical history. **H**, growth of patient 8 PDX in mice treated with vehicle or PLX4720 (45 mg/kg/d orally). Mean tumor volumes \pm SEM ($n = 5$ per group) are shown. **I**, photomicrographs showing H&E staining in tumor (top left), vehicle-treated PDX (top right), PLX4720-treated PDX (bottom left) and a lung metastasis from a PDX-bearing mouse treated with PLX4720 (bottom right) from patient 8. Insets show IHC staining with the melanoma-specific antibody HMB45/MelanA. Scale bar, 100 μ m. **J**, NRAS^{Q61K} allele fraction in DNA from patient 8 blood (germline), and the tumor at baseline and after 12 weeks of vemurafenib. **K**, IGV visualization for WES of codon Q61 of NRAS in the DNA from patient 8 blood (germline), the tumor at 12 weeks and the pleural effusion-PDX at 37 weeks. The percentages indicate the mutant allele fraction in each sample. Green lettering, partial response; orange, stable disease; red, progressive disease; RT, radiotherapy treatment; TT, targeted therapy; IT, immunotherapy; CT, chemotherapy; y, years; SC, subcutaneous; LN, lymph node; RLN, regional lymph node.

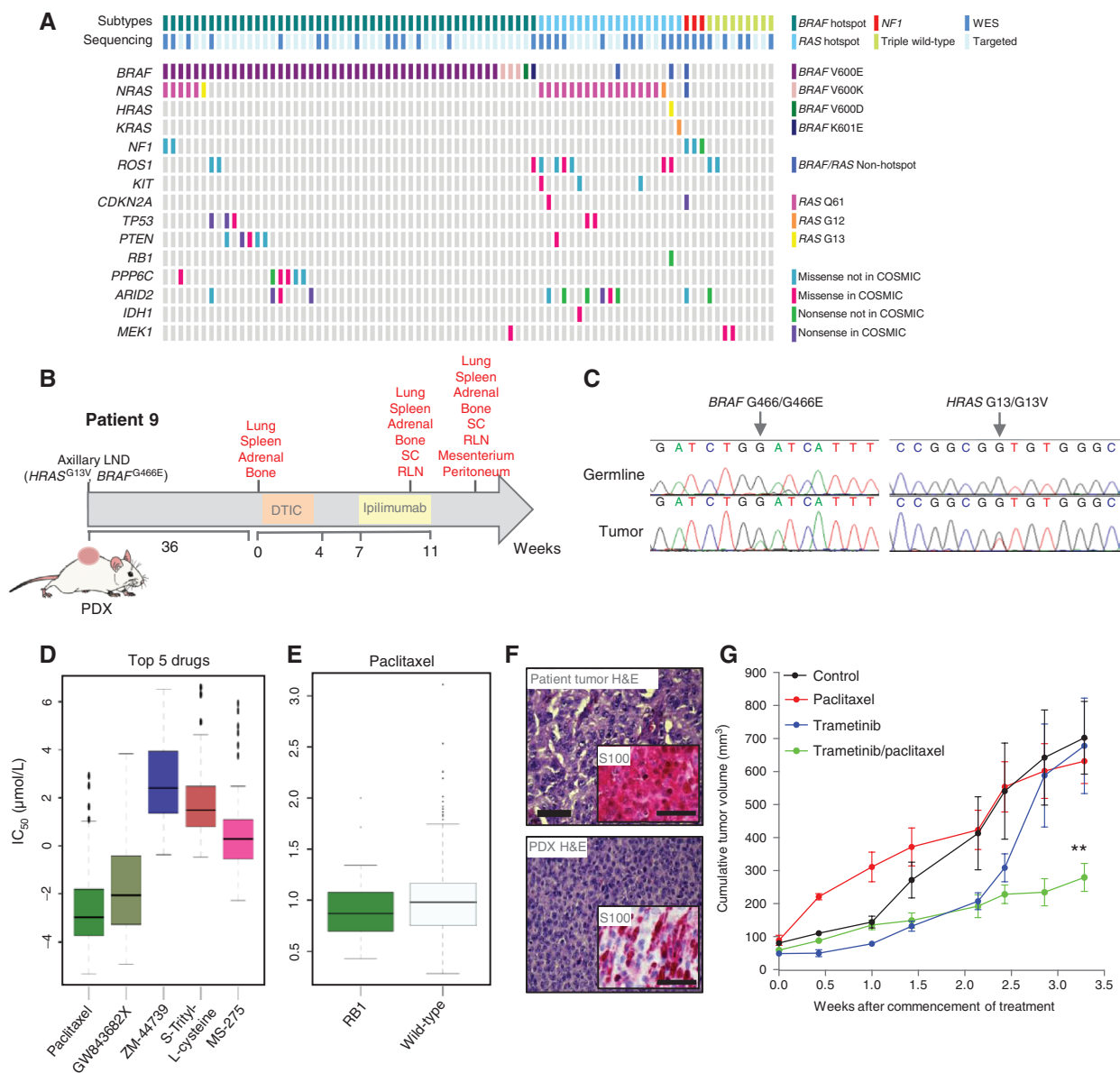


Figure 4. Sequencing and PDX technologies for the identification and validation of therapeutic targets in non-V600 mutant BRAF melanoma. **A**, landscape of driver mutations in 80 malignant melanomas. Top, the mutation subtype (BRAF hotspot, RAS [N/H/K] hotspot, NF1, and triple wild-type) is indicated for each tumor sample. Bottom, color-coded matrix of individual mutations in each sample (specific BRAF and RAS mutations are indicated). **B**, patient 9 clinical history. **C**, Sanger sequencing electropherograms confirming BRAF^{G466E} and HRAS^{G13V} mutations in patient 9. **D**, dose-response curve (or beta) values for RB1 mutant/CNA cell lines screened against the top 5 drugs with increased sensitivity on a RB1-mutated background. Paclitaxel ($n = 60$), GW843682X ($n = 60$), ZM-44739 ($n = 75$), S-Trityl-L-cysteine ($n = 60$), and MS-275 ($n = 63$). **E**, dose-response curve (or beta) values for RB1 mutant/CNA cell lines ($n = 60$) versus RB1 wild-type cell lines ($n = 296$) screened against paclitaxel. $P = 0.0386$ (Mann-Whitney test). **F**, photomicrographs showing H&E staining of the tumor from patient 9 (top) and the corresponding PDX (bottom). Scale bar, 100 μm . Insets show IHC stains with the melanoma marker S100 staining. Scale bar, 100 μm . **G**, growth of PDX from patient 9 in mice treated with vehicle, trametinib (0.15 mg/kg/d orally), paclitaxel (10 mg/kg/d i.p. every third day), or trametinib (0.15 mg/kg/d orally) plus paclitaxel (10 mg/kg/d i.p. every third day). Drug treatments commenced when tumors were $\sim 90 \text{ mm}^3$ and show mean tumor volumes \pm SEM ($n = 7$ per group). Red lettering, progressive disease. RLN, regional lymph node; SC, subcutaneous; DTIC, dacarbazine.

recently defined in the genomic classification of melanoma, and note that the distribution of mutations in these tumors is largely in agreement with that classification (30). Of note, six of the V600 BRAF mutant tumors acquired RAS mutations at resistance (Fig. 4A).

We were intrigued by patient 9 (Fig. 4B), because the tumor presented a rare kinase-dead BRAF mutation (G466E), a rare oncogenic HRAS mutation (G13V; Fig. 4C), and a loss-of-

function RB1 mutation, also rare in melanoma. This unusual constellation of mutations is a therapeutic challenge, because oncogenic RAS drives paradoxical activation of kinase-dead BRAF, so despite the BRAF mutation, BRAF inhibitors will be ineffective (28, 34). The patient originally presented with primary melanoma on the forearm with synchronous regional nodal metastases and was rendered disease-free by surgery, but relapsed after 36 weeks (Fig. 4B). Two cycles of

dacarbazine (DTIC) and one dose of ipilimumab were administered, but a rapidly worsening condition and poor performance status prevented further treatment.

We hypothesized that MEK inhibitors may be effective in this tumor, and it is reported that cells lacking RB1 are sensitive to paclitaxel (ref. 35; Fig. 4D and E), so we tested these drugs in a PDX from the patient's metastatic lesion (Fig. 4B). The PDX retained the histologic features of the patient's tumor (Fig. 4F), and although it did not respond to the MEK inhibitor trametinib or to paclitaxel monotherapies, it was sensitive to the combination of these drugs (Fig. 4G). This demonstrates how PDXs can be used to validate hypothesis-driven combination therapies for patients with melanoma.

Melanoma CTCs Are Tumorigenic

PDXs cannot always be developed if tumors are inaccessible, but we recently demonstrated that xenografts can be established from CTCs in SCLC (23), so we explored if we could develop CDXs from patients with melanoma. We attempted to develop CDXs from 47 blood samples from 40 patients with stage III and IV cutaneous, acral, mucosal, and uveal melanoma (Fig. 5A and Supplementary Table S5) by adapting the SCLC protocol and injecting the enriched CTCs into NSG mice (Fig. 5B). We have been successful in 6 cases, failed in 15, and continue to follow 26 (Fig. 5A), which represents a current success rate of 13%.

A CDX was generated for patient 10, who presented highly aggressive widespread *BRAF*^{V600E} melanoma that was unresponsive to targeted therapy (Fig. 5C). A palpable tumor grew in the first mouse 1 month after cell implantation (F1 CDX), had a doubling time of ~10 days (Fig. 5D), and grew in secondary hosts (F2 CDX; Fig. 5D), demonstrating sustainability. It retained the histopathologic and immunohistochemical features of the patient's tumor and invaded the deep muscular layers (Fig. 5E). The CDX-bearing mice developed lung micrometastases (Fig. 5E), and 2 months after excision of the primary tumor, macroscopic metastases were seen in the liver, lungs, kidneys, lymph nodes, brain, and distant subcutaneous tissue (Fig. 5F and G), and we confirmed that these tumors were metastatic human melanoma by staining for human HMB45/MelanA (Fig. 5G). Thus, the CDX had similar metastatic tropism in mice and the patient, and the cancer cells crossed the blood-brain barrier in both hosts. Copy number aberration (CNA) analysis revealed clear overlap of gains and losses in the patient's tumor and CDX (Fig. 6A), and WES and RNA sequencing revealed extensive concordance of SNVs (Fig. 6B and C). Notably, coincident with the patient's lack of response to dabrafenib, the CDX also failed to respond to this drug, showing only a 2-week delay in growth (Fig. 6D).

We also developed a CDX from patient 11, who presented extensive metastases in retrocaval lymph nodes and acute bowel obstruction. A *BRAF*^{V600E} mutation was confirmed and the patient commenced vemurafenib, but was switched to dabrafenib due to skin toxicity (Fig. 6E). The CDX from this patient, established at week 2, developed in ~2.5 months (F1 CDX), had a doubling time of ~10 days (Fig. 6F), and grew in secondary hosts (F2 CDX; Fig. 6F). It retained the histopathologic and immunohistochemical features of the patient's tumor and metastasized to the lungs (Fig. 6G). Moreover, following excision of the primary tumor, we observed widespread macroscopic disease in the mouse hosts (Fig. 6H), and,

coincident with the patient's short response to vemurafenib and dabrafenib, the CDX presented a short-lived response to PLX4720 (Fig. 6I). Thus, we describe the development of melanoma CDXs, a new tool to study melanoma biology in patients with advanced-stage disease, and for monitoring and predicting patient responses to therapy when tumors are inaccessible.

DISCUSSION

There have been enormous advances in the management of melanoma over the past 5 years. New targeted therapies and immunotherapies have improved progression-free and overall survival in this disease, and in some cases led to cures. However, resistance emerges in the majority of patients on targeted therapies and not all patients respond to immunotherapies, so it is clinically challenging to select patients for these different modalities, to determine when to switch between modalities and to select second-line therapies for patients who fail to respond or who relapse. Here, we describe systematic analysis of patient samples to improve the personalization of targeted therapies and immunotherapies. We argue that no single approach allows refinement of care in all patients and that integration of data from a platform of technologies that interrogates different aspects of tumor biology is needed to select the most appropriate treatment for an individual patient. Clearly, these analyses need to be conducted in a timely manner so that treatment can be refined to ensure the best possible outcome.

It has been shown that ctDNA is a reliable, inexpensive, and minimally invasive technique that allows assessment of response to therapy in breast and colorectal cancers (21, 36–38). This technology was previously explored in a small number of patients with melanoma (39–41), primarily through application of mutation-specific droplet digital PCR assays. We extend those studies by establishing that next-generation sequencing of ctDNA can be used as a routine clinical tool to monitor patient responses to treatment, but also to reveal mechanisms of resistance even in the absence of prior knowledge of the underlying molecular processes. We showed that longitudinal monitoring of *BRAF* and *NRAS* driver mutations could be used to prospectively follow patient responses to targeted therapy and immunotherapy. In agreement with previous studies, we show that ctDNA generally revealed the disease course earlier than imaging, and we show that it was more accurate at predicting responses than serum LDH. Moreover, although LDH can be prognostic in melanoma (42), its levels can increase in unrelated conditions such as liver disease and myocardial infarction (43), which can confound interpretation of therapy responses. The potential of ctDNA was demonstrated in patient 4, where the results initially appeared discordant because *NRAS*^{Q61R} was undetectable when the CT scan showed progressive disease. However, a subsequent scan revealed tumor shrinkage, demonstrating that ctDNA had accurately predicted this delayed response to immunotherapy. A similar observation was recently reported in another patient with a delayed immunotherapy response (44), so together these data suggest that ctDNA could be particularly valuable in patients with delayed responses to immunotherapy.

We were intrigued that the *BRAF*-mutant variant allele fraction (VAF) was consistently higher than the mutant VAFs that mediated resistance. One possible explanation for this is

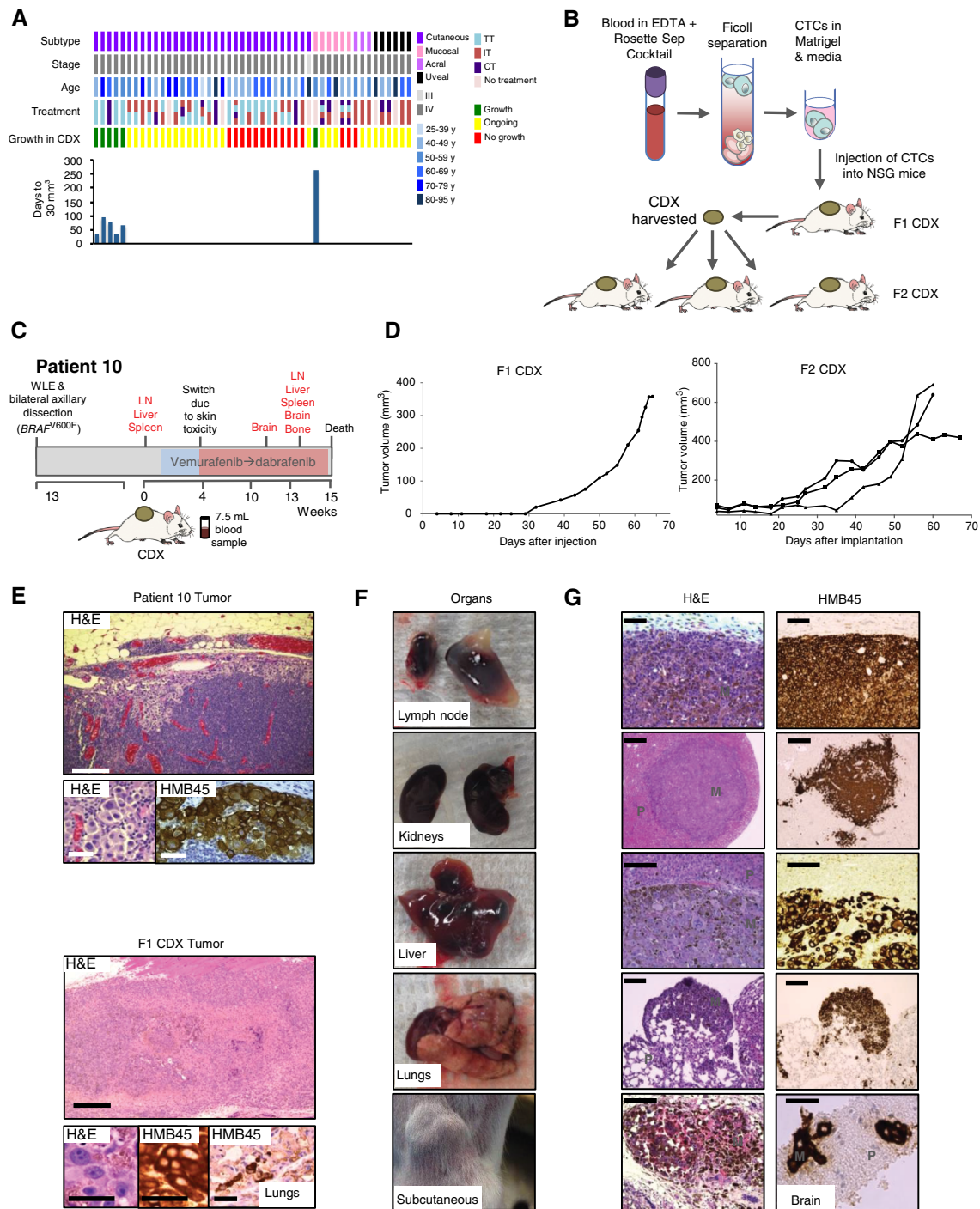


Figure 5. Melanoma CDXs are a tool for personalized medicine in advanced disease. **A**, overview of CTCs isolated from 47 blood samples from 40 patients with cutaneous, acral, and uveal melanoma implanted into NSG mice to establish CDXs (see Supplementary Materials for more information on melanoma patient sample classification). **B**, generation of CDX models by CTC enrichment and s.c. injection in NSG mice. **C**, patient 10 clinical history. Red lettering indicates progressive disease at the indicated locations. **D**, growth of F1 and F2 CDXs in NSG mice. **E**, H&E histologic image of the tumor from patient 10 (top) and the corresponding F1 CDX (bottom). Top, H&E image of the patient tumor (upper image; scale bars, 300 μ m) and high power magnification H&E and IHC staining with HMB45/MelanA from metastatic lesions in the patient's regional lymph node (bottom images; scale bars, 20 μ m). Lower, H&E image of the F1 CDX tumor (upper image; scale bars, 300 μ m) and high-power magnification H&E and IHC staining for HMB45/MelanA of a metastatic deposit in the mouse lung (scale bars, 25 μ m). **F**, photographs of lymph nodes, kidneys, liver, lungs, and skin (subcutaneous tumor) showing macroscopic metastasis in the visceral organs of F2 CDX-bearing mice. **G**, H&E photomicrographs and IHC staining for HMB45/MelanA of the metastatic lesions in the visceral organs of the F2 CDX mice. M, metastasis; P, normal tissue parenchyma. All scale bars 150 μ m except bottom lowest image, 20 μ m. Red lettering, progressive disease; TT, targeted therapy; IT, immunotherapy; CT, chemotherapy.

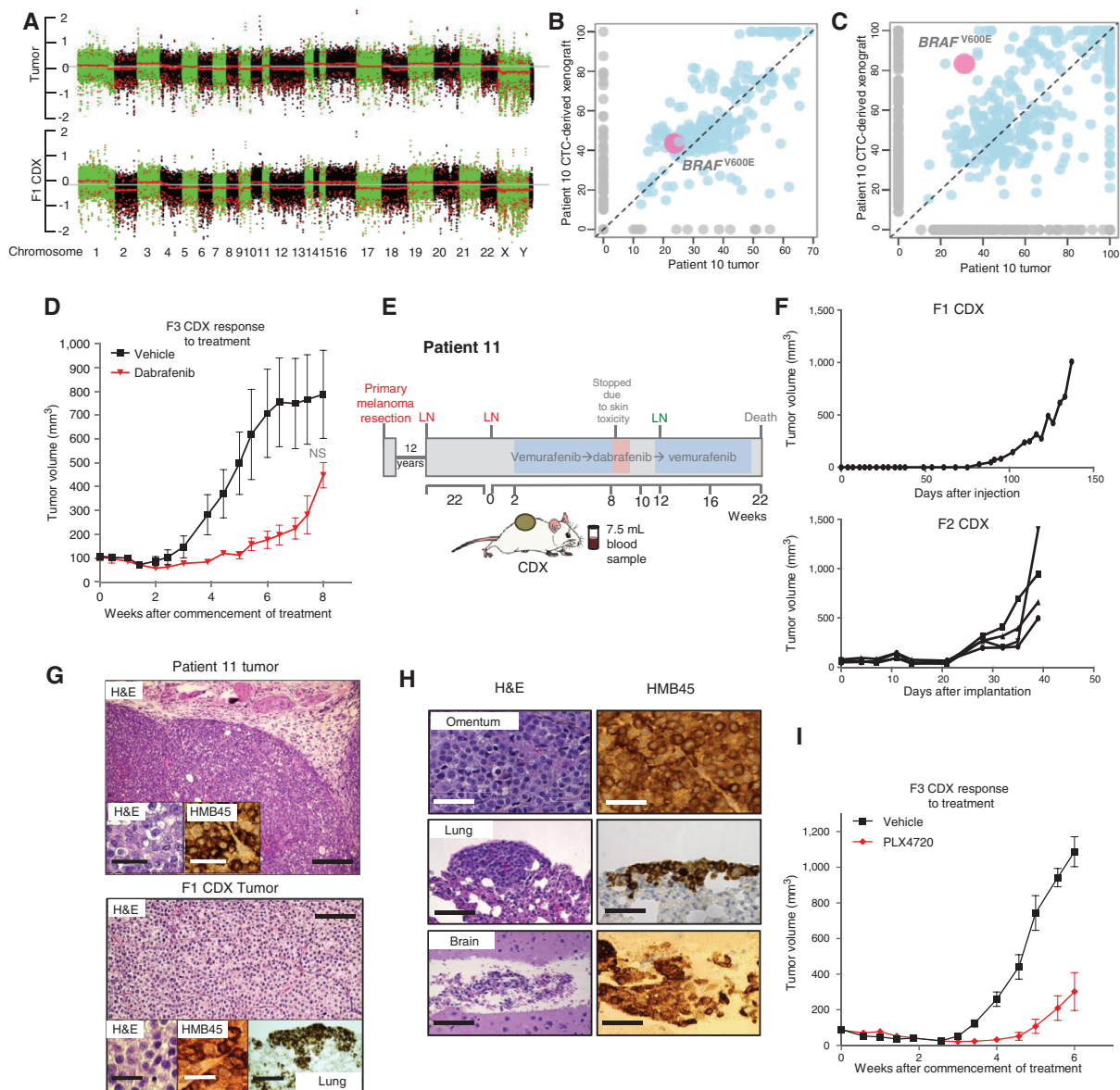


Figure 6. CDXs are representative of human tumors. **A**, CNA analysis of the patient 10 tumor and F1 CDX. **B**, VAF expressed in percentage in tumor and F1 CDX. Gray dots, private SNVs; blue dots, shared SNVs; pink dot, *BRAF*^{V600E}. Dotted line, ideal fit. Pearson product-moment correlation $P < 2.2 \times 10^{-16}$; $r^2 = 0.67$. **C**, allele fraction plot expressed in percentage from RNA sequencing of patient tumor and F1 CDX. **D**, growth of patient 10 F3 CDX in mice treated with vehicle or dabrafenib (25 mg/kg/d orally). Mean volumes \pm SEM are shown ($n = 6$ per group). n.s., nonsignificant (t test, two-sided). **E**, patient 11 clinical history. Red lettering, progressive disease at the indicated locations. LN, lymph node. **F**, growth of the F1 CDX and F2 CDX in individual NSG mice. **G** (top), patient 11 regional lymph node metastasis H&E photomicrograph (scale bar, 150 μ m); inset (left), high power magnification H&E (scale bar, 25 μ m); inset right, IHC staining with HMB45/MelanA (scale bar, 25 μ m). Bottom, F1 CDX tumor H&E photomicrograph (scale bar, 100 μ m); inset left, high power magnification H&E (scale bar, 20 μ m); inset center, F1 CDX tumor IHC staining with HMB45/MelanA (scale bar, 20 μ m); inset right, lung metastasis IHC staining with HMB45/MelanA (scale bar, 200 μ m). **H**, H&E photomicrographs (left) and IHC staining with HMB45/MelanA (right) of the visceral metastases in F2 CDX mice. Scale bars: top row, 30 μ m; mid row, 100 μ m; bottom row left, 100 μ m; bottom row right, 40 μ m. **I**, growth of patient 11 F3 CDX in mice treated with vehicle or PLX4720 (45 mg/kg/d orally). Mean volumes \pm SEM are shown ($n = 6$ per group).

that resistance was mediated by several subclones driven by distinct mechanisms, so although all subclones contributed to the *BRAF*-mutant ctDNA, each contributed only partially to the resistance mutant ctDNA pool. An alternative possibility is that cells treated with targeted therapies secrete factors that promote the survival of drug-sensitive cells (45), suggesting that resistant cells can sustain sensitive cells and therefore persist as a minority population in the resistant tumor.

Our study shows that ctDNA is a tractable biomarker that can assist clinical decisions in a variety of settings. We advocate that *BRAF* and *NRAS* ctDNA are monitored and further validated in prospective clinical trials and they now have a part in routine clinical practice. With targeted therapies, an increase in *BRAF*-mutant VAF will provide an early warning of progression, and the *NRAS* analysis will reveal mechanisms of resistance in approximately 30% of patients (32). In particular,

this technique could be used to prioritize patients for scans, so that disease progression can be confirmed early and patient care adjusted at the earliest opportunity. Over and above the benefits for individual patients, the use of ctDNA should allow treatment selection to be more cost effective, allowing more timely and accurate decision making on when to start or stop treatment with these very expensive drugs.

We show that PDX technologies can complement ctDNA analysis to optimize patient care. Support for the predictive power of PDXs has been shown in a small number of clinical cases (22, 46, 47), although limitations of PDX models due to tumor heterogeneity and interspecies compatibility have also been noted (48, 49). Critically, our PDX models were established with a median latency of 49 days, and we show that this provided sufficient time to test clinically relevant questions for numerous patients in this study. A central component of the potential of PDXs is the rapid analysis of the genomic landscape of tumors. We show that WES of the tumors allowed the identification of genetic alterations beyond *BRAF* hotspot mutations and, in combination with PDX models, allowed the selection and validation of first-line and second-line treatments. We show that integration of WES and ctDNA sequencing with functional studies in PDXs provides a powerful combination that can change clinical practice and improve patient outcomes.

For one of our patients, WES revealed that trametinib plus paclitaxel may have been effective, and we validated this combination in the patient's PDX. Notably, a phase I clinical trial with combination trametinib/paclitaxel (PAC-MEL) reported ~40% partial response rates in patients with non-V600 mutant *BRAF* (50), but no molecular mechanisms were provided to explain the responses. Our data may provide a foundation for patient stratification with this combination, validating the clinical relevance of our approach. Moreover, the approach is particularly relevant for umbrella and basket trials, where preclinical evaluation of drug efficiency or combinations in individual patient tumors could assist optimization of patient benefit and cost. We also show that this technology may assist in decisions about when to treat beyond relapse for some patients. A limitation of the approach is access to new agents to test in PDX models, or to administer to the patients, but linking drugs to real-time PDX data clearly has the potential to improve patient care and outcomes. We strongly advocate that PDXs be established as early as possible during patient care to allow as much time as possible for these studies to be conducted.

It is difficult to apply PDX technology to patients with very advanced disease who have exhausted conventional treatment options, as carrying out a biopsy solely to access fresh tumor for investigational techniques may not be considered to be in their best interest. Thus, although it is important to study late-stage disease biology, samples are difficult to obtain. We show that this limitation can be overcome in some patients by CDX techniques. We establish a proof-of-principle for this approach in melanoma and show that the CDXs resemble patient tumors and response to therapies. Our data establish that melanoma CTCs are tumorigenic and that they have similar tropism to the patient's own tumors. Because it is not currently possible to reliably quantify CTCs in melanoma, we cannot correlate CTC count to the successful establishment of CDXs, but we note that in all six cases where CDXs were established, the patients had

widespread, late-stage disease, suggesting that this approach is more successful in patients with high disease burden. Thus, we establish that CDX technology is feasible in melanoma, and this approach is particularly important when patient tumors are inaccessible or difficult to biopsy. Clearly, this technology provides an opportunity to study late-stage disease.

In summary, we describe integration of WES, ctDNA analysis, PDX, and CDX technologies as a powerful platform to optimize clinical management of patients with melanoma. We emphasize that it is not feasible to use all of these approaches in all patients but, nevertheless, careful selection of relevant components can be used to improve individual patient care. PDXs did not grow for ~30% of patients, and the take rate for CDXs was considerably lower, but the ctDNA still revealed responses to treatment and provided early warning of relapse in most patients. Moreover, WES or targeted sequencing of ctDNA provided insight into mechanisms of resistance in many patients. Our aim was to develop a pipeline to improve patient care, and for at least 1 patient we obtained a treatment that was not otherwise available. This shows the power of our approach, and we are now further refining our platform to enable us to optimize care for the majority of patients.

METHODS

See Supplementary Materials for full details.

Patients and Samples

Patients were managed in accordance with the ethical principles originating from the Declaration of Helsinki and in accordance with Good Clinical Practice as defined by the International Conference on Harmonisation. All patients were treated according to standard clinical protocols or as part of clinical trials approved by our Institutional Review Board. Standard treatments included, where appropriate, access to treatments available through Medicines Health Regulatory Agency (MHRA)-approved Expanded Access Programs (EAP) or Early Access to Medicines Schemes (EAMS). All patients gave informed written consent to participate in clinical trials or EAP or EAMS. Patient samples were collected with written full-informed patient consent under Manchester Cancer Research Centre (MCRC) Biobank ethics application #07/H1003/161+5 and approval for the work under MCRC Biobank Access Committee application 13_RIMA_01.

Animal Procedures

All procedures involving animals were performed in accordance with ARRIVE guidelines and National Home Office regulations under the Animals (Scientific Procedures) Act 1986 and within guidelines set out by the Cancer Research UK Manchester Institute's Animal Ethics Committee and the Committee of the National Cancer Research Institute at The Institute of Cancer Research Animal Welfare and Ethical Review Body, and carried out under licenses PPL-70/7635 and PPL-70/7701.

Blood Processing and Circulating Cell-Free DNA Extraction

Blood was collected into BD Vacutainer K2E (EDTA) tubes (Becton-Dickinson), double centrifuged at $2,000 \times g$ for 10 minutes at room temperature, and the plasma stored at -80°C within 4 hours of collection. Circulating cell-free DNA (cfDNA) was extracted with QIAamp Circulating Nucleic Acid Kits (Qiagen) per the manufacturer's instructions, quantified by the TaqMan RNaseP Assay (Life Technologies) and stored at -80°C . LDH was determined independently by the Christie Pathology Laboratories.

WES of ctDNA and Tumor Samples

WES on solid tumors was performed as previously described (51). For cfDNA sequencing, a library was generated using 13 ng of cfDNA in an Accel-NGS 2S DNA Library Kit for the Illumina Platform (Swift Biosciences) according to the manufacturer's instructions, with small modifications (see Supplementary Materials).

NGS Mutation Detection

For retrospective analyses, the DNA loci corresponding to *NRAS*^{Q61} and *BRAF*^{V600} were quantified following PCR amplification of a 120-bp *NRAS* fragment and 108-bp *BRAF* fragment from 1 ng of patient cfDNA (*NRAS*^{Q61}: forward primer 5'-GTATTGGTCTCTCATGGCACTGT, reverse primer 5'-TACCCTCCACACCCAG; *BRAF*^{V600}: forward primer 5'-TTCATGAAGACCTCACAGTAAAA, reverse primer 5'-TCCACAAAATGGATCCAGAC). For subsequent prospective analysis a targeted 10-loci PCR panel was used (Supplementary Table S2). PCR products were gel purified using QIAquick Gel Extraction Kits (Qiagen) and quantified using Qubit 2.0 Fluorometer (Life Technologies). Five nanograms of each purified PCR product (for retrospective analyses) or 250 ng of the multiplexed PCR product (for prospective analyses) were cloned into a NEBNext Ultra DNA Library Prep Kit for Illumina (New England Biolabs) according to the manufacturer's instructions. Following purification and quantification, libraries were mixed with 35% PhiX Control v3 (Illumina) or multiplexed with sequencing libraries of higher complexity to facilitate clustering and processed on an Illumina MiSeq (Illumina).

Real-time PCR Mutation Detection

BRAF (V600E, c.1799T>A) and *NRAS* (*NRAS*^{Q61K}, c.181C>A, *NRAS*^{Q61R}, c.182A>G and *NRAS*^{Q61L}, c.182A>T) mutations were detected using castPCR assays (Life Technologies) according to the manufacturer's instructions. Briefly, 4 μ L of genomic DNA (0.71–40 ng) was combined with 10 μ L TaqMan Gene Expression Master Mix and 2 μ L mutation-specific or *NRAS* reference primer and probes. Genomic DNA isolated from A375 melanoma cells and DNA isolated from whole blood of two patients with melanoma carrying confirmed *NRAS* wild-type tumors were used to establish Detection Δ C_T Cutoff values. All reactions were processed on an ABI 7900HT Real-time PCR machine and analyzed using SDS 2.4 software (Life Technologies).

Establishing Patient-Derived Xenografts

Patient tumor samples (~80 mm³) were implanted subcutaneously in 6-week-old female NSG mice. All animals were dosed by daily orogastric gavage with drug or vehicle (5% DMSO in water). For patient 5, animals were randomized into groups receiving PLX4720 (45 mpk) or vehicle for 120 days. Tumors were passaged into additional mice, and the animals randomized for treatment with PLX4720 (45 mpk) or dabrafenib (25 mpk)/trametinib (0.15 mpk). For patient 8, animals were randomized before initiation of treatment with PLX4720 (45 mpk) or vehicle for 34 days. For patient 9, animals were randomized for daily orogastric gavage treatment with vehicle, trametinib (0.15 mpk) and/or intraperitoneal administration of paclitaxel (20 mpk) twice a week. For patient 10, animals were randomized for treatment with dabrafenib (25 mpk) or vehicle for 56 days. For patient 11, animals were randomized for treatment with PLX4720 (45 mpk) or vehicle for 42 days.

CTC-Derived Xenografts

Methods used have been previously described (23).

Disclosure of Potential Conflicts of Interest

G. Brady is a consultant/advisory board member for Epistem. P. Lorigan reports receiving speakers bureau honoraria from Bristol-Myers Squibb, Merck, Novartis, and Roche; is a consultant/advisory board member for Amgen, Bristol-Myers Squibb, GlaxoSmithKline,

Merck, Novartis, and Roche; and has provided expert testimony for Bristol-Myers Squibb, Merck, and Roche. R. Marais reports receiving speakers bureau honoraria from the GlaxoSmithKline special symposium at the SMR Congress 2015 and has ownership interest in a *BRAF* gene patent, payment from Wellcome Trust, part of research team while at The Institute for Cancer Research. No potential conflicts of interest were disclosed by the other authors.

Authors' Contributions

Conception and design: M.R. Girotti, G. Gremel, P. Lorigan, R. Marais
Development of methodology: M.R. Girotti, G. Gremel, R. Lee, E. Galvani, K.H.J. Lim, G. Brady, P. Lorigan, C. Dive

Acquisition of data (provided animals, acquired and managed patients, provided facilities, etc.): M.R. Girotti, G. Gremel, R. Lee, E. Galvani, D. Rothwell, A. Viros, F. Baenke, M. Pedersen, J. Swan, A. Fusi, D. Oudit, P. Lorigan, C. Dive, R. Marais

Analysis and interpretation of data (e.g., statistical analysis, biostatistics, computational analysis): M.R. Girotti, G. Gremel, E. Galvani, A. Viros, A.K. Mandal, S.J. Furney, M. Pedersen, A. Fusi, P. Lorigan, C. Dive, R. Marais

Writing, review, and/or revision of the manuscript: M.R. Girotti, G. Gremel, R. Lee, K.H.J. Lim, N. Dhomen, P. Lorigan, C. Dive, R. Marais

Administrative, technical, or material support (i.e., reporting or organizing data, constructing databases): M.R. Girotti, R. Lee, A.K. Mandal, K.H.J. Lim, G. Saturno, J. Rogan, M. Smith, A. Fusi, N. Dhomen, R. Marais

Study supervision: G. Brady, P. Lorigan, R. Marais

Other [provided expertise in circulating biomarkers (ctDNA) and CDX protocols]: C. Dive

Acknowledgments

The authors thank the patients and their families. They also thank Dr. Cassandra Hodgkinson for advice.

Grant Support

This work was supported by the CRUK Manchester Institute (C5759/A20971) and the Wellcome Trust (100282/Z/12/Z).

Received November 9, 2015; revised December 20, 2015; accepted December 23, 2015; published OnlineFirst December 29, 2015.

REFERENCES

1. <http://www.Cancer.org>. Accessed February 3, 2016.
2. Ferlay J, Steliarova-Foucher E, Lortet-Tieulent J, Rosso S, Coebergh JW, Comber H, et al. Cancer incidence and mortality patterns in Europe: estimates for 40 countries in 2012. *Eur J Cancer* 2013;49:1374-403.
3. Chapman PB, Hauschild A, Robert C, Haanen JB, Ascierto P, Larkin J, et al. Improved survival with vemurafenib in melanoma with BRAF V600E mutation. *N Engl J Med* 2011;364:2507-16.
4. Flaherty KT, Infante JR, Daud A, Gonzalez R, Kefford RF, Sosman J, et al. Combined BRAF and MEK inhibition in melanoma with BRAF V600 mutations. *N Engl J Med* 2012;367:1694-703.
5. Sosman JA, Kim KB, Schuchter L, Gonzalez R, Pavlick AC, Weber JS, et al. Survival in BRAF V600-mutant advanced melanoma treated with vemurafenib. *N Engl J Med* 2012;366:707-14.
6. Girotti MR, Pedersen M, Sanchez-Laorden B, Viros A, Turajlic S, Niculescu-Duvaz D, et al. Inhibiting EGF receptor or SRC family kinase signaling overcomes BRAF inhibitor resistance in melanoma. *Cancer Discov* 2013;3:158-67.
7. Larkin J, Ascierto PA, Dreno B, Atkinson V, Liskay G, Maio M, et al. Combined vemurafenib and cobimetinib in BRAF-mutated melanoma. *N Engl J Med* 2014;371:1867-76.
8. Long GV, Stroyakovskiy D, Gogas H, Levchenko E, de Braud F, Larkin J, et al. Combined BRAF and MEK inhibition versus BRAF inhibition alone in melanoma. *N Engl J Med* 2014;371:1877-88.

9. Girotti MR, Saturno G, Lorigan P, Marais R. No longer an untreatable disease: How targeted and immunotherapies have changed the management of melanoma patients. *Mol Oncol* 2014;8:1140–58.
10. Larkin J, Chiarion-Sileni V, Gonzalez R, Grob JJ, Cowey CL, Lao CD, et al. Combined nivolumab and ipilimumab or monotherapy in untreated melanoma. *N Engl J Med* 2015;373:23–34.
11. Robert C, Schachter J, Long GV, Arance A, Grob JJ, Mortier L, et al. Pembrolizumab versus ipilimumab in advanced melanoma. *N Engl J Med* 2015;372:2521–32.
12. Snyder A, Makarov V, Merghoub T, Yuan J, Zaretsky JM, Desrichard A, et al. Genetic basis for clinical response to CTLA-4 blockade in melanoma. *N Engl J Med* 2014;371:2189–99.
13. Tumeah PC, Harview CL, Yearley JH, Shintaku IP, Taylor EJ, Robert L, et al. PD-1 blockade induces responses by inhibiting adaptive immune resistance. *Nature* 2014;515:568–71.
14. Ackerman A, Klein O, McDermott DF, Wang W, Ibrahim N, Lawrence DP, et al. Outcomes of patients with metastatic melanoma treated with immunotherapy prior to or after BRAF inhibitors. *Cancer* 2014;120:1695–701.
15. Chan M, Haydu L, Menzies AM, Azer MWF, Klein O, Guminski A, et al. Clinical characteristics and survival of BRAF-mutant (BRAF+) metastatic melanoma patients (pts) treated with BRAF inhibitor (BRAFi) dabrafenib or vemurafenib beyond disease progression (PD). *J Clin Oncol* 31, 2013 (suppl; abstr 9062).
16. Stratton MR. Exploring the genomes of cancer cells: progress and promise. *Science* 2011;331:1553–8.
17. Garnett MJ, Edelman EJ, Heidorn SJ, Greenman CD, Dastur A, Lau KW, et al. Systematic identification of genomic markers of drug sensitivity in cancer cells. *Nature* 2012;483:570–5.
18. Yang W, Soares J, Greninger P, Edelman EJ, Lightfoot H, Forbes S, et al. Genomics of Drug Sensitivity in Cancer (GDSC): a resource for therapeutic biomarker discovery in cancer cells. *Nucleic Acids Res* 2013;41:D955–61.
19. Shi H, Hugo W, Kong X, Hong A, Koya RC, Moriceau G, et al. Acquired resistance and clonal evolution in melanoma during BRAF inhibitor therapy. *Cancer Discov* 2014;4:80–93.
20. Chan KC, Jiang P, Zheng YW, Liao GJ, Sun H, Wong J, et al. Cancer genome scanning in plasma: detection of tumor-associated copy number aberrations, single-nucleotide variants, and tumoral heterogeneity by massively parallel sequencing. *Clin Chem* 2013;59:211–24.
21. Murtaza M, Dawson SJ, Tsui DW, Gale D, Forshew T, Piskorz AM, et al. Non-invasive analysis of acquired resistance to cancer therapy by sequencing of plasma DNA. *Nature* 2013;497:108–12.
22. Einarsdottir BO, Bagge RO, Bhadury J, Jespersen H, Mattsson J, Nilsson LM, et al. Melanoma patient-derived xenografts accurately model the disease and develop fast enough to guide treatment decisions. *Oncotarget* 2014;5:9609–18.
23. Hodgkinson CL, Morrow CJ, Li Y, Metcalf RL, Rothwell DG, Trapani F, et al. Tumorigenicity and genetic profiling of circulating tumor cells in small-cell lung cancer. *Nat Med* 2014;20:897–903.
24. <http://www.ema.europa.eu.WC500021864-8.pdf>. Accessed December 16, 2015.
25. Girotti MR, Lopes F, Preece N, Niculescu-Duvaz D, Zambon A, Davies L, et al. Paradox-breaking RAF inhibitors that also target SRC are effective in drug-resistant BRAF mutant melanoma. *Cancer Cell* 2015;27:85–96.
26. Su F, Viros A, Milagre C, Trunzer K, Bollag G, Spleiss O, et al. RAS mutations in cutaneous squamous-cell carcinomas in patients treated with BRAF inhibitors. *N Engl J Med* 2012;366:207–15.
27. Johnson DB, Flaherty KT, Weber JS, Infante JR, Kim KB, Kefford RF, et al. Combined BRAF (Dabrafenib) and MEK inhibition (Trametinib) in patients with BRAFV600-mutant melanoma experiencing progression with single-agent BRAF inhibitor. *J Clin Oncol* 2014;32:3697–704.
28. Heidorn SJ, Milagre C, Whittaker S, Nourry A, Niculescu-Duvaz I, Dhomen N, et al. Kinase-dead BRAF and oncogenic RAS cooperate to drive tumor progression through CRAF. *Cell* 2010;140:209–21.
29. Sanchez-Laorden B, Viros A, Girotti MR, Pedersen M, Saturno G, Zambon A, et al. BRAF inhibitors induce metastasis in RAS mutant or inhibitor-resistant melanoma cells by reactivating MEK and ERK signaling. *Sci Signal* 2014;7:ra30.
30. Cancer Genome Atlas Network. Genomic classification of cutaneous melanoma. *Cell* 2015;161:1681–96.
31. Hodis E, Watson IR, Kryukov GV, Arold ST, Imielinski M, Theurillat JP, et al. A landscape of driver mutations in melanoma. *Cell* 2012;150:251–63.
32. Van Allen EM, Wagle N, Sucker A, Treacy DJ, Johannessen CM, Goetz EM, et al. The genetic landscape of clinical resistance to RAF inhibition in metastatic melanoma. *Cancer Discov* 2014;4:94–109.
33. Busser B, Leccia MT, Gras-Combe G, Bricaut I, Templier I, Claeys A, et al. Identification of a novel complex BRAF mutation associated with major clinical response to vemurafenib in a patient with metastatic melanoma. *JAMA Dermatol* 2013;149:1403–6.
34. Pedersen M, Viros A, Cook M, Marais R. (G12D) NRAS and kinase-dead BRAF cooperate to drive naevogenesis and melanomagenesis. *Pigment Cell Melanoma Res* 2014;27:1162–6.
35. <http://www.cancerrxgene.org>. Accessed August 6, 2014.
36. Bettegowda C, Sausen M, Leary RJ, Kinde I, Wang Y, Agrawal N, et al. Detection of circulating tumor DNA in early- and late-stage human malignancies. *Sci Transl Med* 2014;6:224ra24.
37. Dawson SJ, Tsui DW, Murtaza M, Biggs H, Rueda OM, Chin SF, et al. Analysis of circulating tumor DNA to monitor metastatic breast cancer. *N Engl J Med* 2013;368:1199–209.
38. Garcia-Murillas I, Schiavon G, Weigelt B, Ng C, Hrebien S, Cutts RJ, et al. Mutation tracking in circulating tumor DNA predicts relapse in early breast cancer. *Sci Transl Med* 2015;7:302ra133.
39. Chang-Hao Tsao S, Weiss J, Hudson C, Christophi C, Cebon J, Behren A, et al. Monitoring response to therapy in melanoma by quantifying circulating tumour DNA with droplet digital PCR for BRAF and NRAS mutations. *Sci Rep* 2015;5:11198.
40. Lipson EJ, Velculescu VE, Pritchard TS, Sausen M, Pardoll DM, Topalian SL, et al. Circulating tumor DNA analysis as a real-time method for monitoring tumor burden in melanoma patients undergoing treatment with immune checkpoint blockade. *J Immunother Cancer* 2014;2:42.
41. Oxnard GR, Pawletz CP, Kuang Y, Mach SL, O'Connell A, Messineo MM, et al. Noninvasive detection of response and resistance in EGFR-mutant lung cancer using quantitative next-generation genotyping of cell-free plasma DNA. *Clin Cancer Res* 2014;20:1698–705.
42. Balch CM, Gershenwald JE, Soong SJ, Thompson JF, Atkins MB, Byrd DR, et al. Final version of 2009 AJCC melanoma staging and classification. *J Clin Oncol* 2009;27:6199–206.
43. Wroblewski F, Gregory KF. Lactic dehydrogenase isozymes and their distribution in normal tissues and plasma and in disease states. *Ann N Y Acad Sci* 1961;94:912–32.
44. Gray ES, Rizos H, Reid AL, Boyd SC, Pereira MR, Lo J, et al. Circulating tumor DNA to monitor treatment response and detect acquired resistance in patients with metastatic melanoma. *Oncotarget* 2015;6:42008–18.
45. Obenauf AC, Zou Y, Ji AL, Vanharanta S, Shu W, Shi H, et al. Therapy-induced tumour secretomes promote resistance and tumour progression. *Nature* 2015;520:368–72.
46. Guerreschi P, Scalbert C, Qassemayr A, Kluza J, Ravasi L, Huglo D, et al. Patient-derived tumor xenograft model to guide the use of BRAF inhibitors in metastatic melanoma. *Melanoma Res* 2013;23:373–80.
47. Whittle JR, Lewis MT, Lindeman GJ, Visvader JE. Patient-derived xenograft models of breast cancer and their predictive power. *Breast Cancer Res* 2015;17:17.
48. Cassidy JW, Caldas C, Bruna A. Maintaining tumor heterogeneity in patient-derived tumor xenografts. *Cancer Res* 2015;75:2963–8.
49. Tentler JJ, Tan AC, Weekes CD, Jimeno A, Leong S, Pitts TM, et al. Patient-derived tumour xenografts as models for oncology drug development. *Nat Rev Clin Oncol* 2012;9:338–50.
50. Coupe N, Corrie P, Hategan M, Larkin J, Gore M, Gupta A, et al. PACMEL: a phase 1 dose escalation trial of trametinib (GSK1120212) in combination with paclitaxel. *Eur J Cancer* 2015;51:359–66.
51. Turajlic S, Furney SJ, Stamp G, Rana S, Ricken G, Oduko Y, et al. Whole-genome sequencing reveals complex mechanisms of intrinsic resistance to BRAF inhibition. *Ann Oncol* 2014;25:959–67.

CANCER DISCOVERY

Application of Sequencing, Liquid Biopsies, and Patient-Derived Xenografts for Personalized Medicine in Melanoma

Maria Romina Girotti, Gabriela Gremel, Rebecca Lee, et al.

Cancer Discov 2016;6:286-299. Published OnlineFirst December 29, 2015.

Updated version	Access the most recent version of this article at: doi: 10.1158/2159-8290.CD-15-1336
Supplementary Material	Access the most recent supplemental material at: http://cancerdiscovery.aacrjournals.org/content/suppl/2015/12/29/2159-8290.CD-15-1336.DC1.html

Cited articles	This article cites 47 articles, 14 of which you can access for free at: http://cancerdiscovery.aacrjournals.org/content/6/3/286.full.html#ref-list-1
-----------------------	--

Citing articles	This article has been cited by 5 HighWire-hosted articles. Access the articles at: /content/6/3/286.full.html#related-urls
------------------------	---

E-mail alerts	Sign up to receive free email-alerts related to this article or journal.
----------------------	--

Reprints and Subscriptions	To order reprints of this article or to subscribe to the journal, contact the AACR Publications Department at pubs@aacr.org .
-----------------------------------	--

Permissions	To request permission to re-use all or part of this article, contact the AACR Publications Department at permissions@aacr.org .
--------------------	---